PHYSICAL REVIEW A **96**, 043852 (2017)

# Scattering properties of a $\mathcal{PT}$ dipole

K. Staliunas,[1,2] P. Markoš,[3] and V. Kuzmiak[4]
[1]*Department de Física i Egineria Nuclear, Universitat Politècnica de Catalunya (UPC), Barcelona 08222, Terrassa, Spain*
[2]*Institució Catalana de Recercai Estudis Avanats (ICREA), Barcelona 08010, Spain*
[3]*Department of Experimental Physics, Faculty of Mathematics Physics and Informatics, Comenius University in Bratislava, 842 28, Slovakia*
[4]*The Czech Academy of Sciences, Institute of Photonics and Electronics, Chaberska 57, 182 51, Praha 8, Czech Republic*
(Received 28 July 2017; published 23 October 2017)

Electromagnetic response of a $\mathcal{PT}$ dipole is studied both analytically and numerically. In the analytical approach, the dipole is represented by two point scatterers. Within the first Born approximation, the asymmetry of the scattering field with respect to the orientation of the dipole is proven. In numerical simulations, the dipole is represented by two infinitely long, parallel cylinders with opposite sign of the imaginary part of a refractive index. Numerical data confirm the validity of the Born approximation in the weak scattering limit, while significant deviations from the Born approximation were observed for stronger scatterers and in the near-field range.

DOI: 10.1103/PhysRevA.96.043852

## I. INTRODUCTION

Parity-time ($\mathcal{PT}$) symmetry has recently emerged as a promising design principle for extending Hermitian to non-Hermitian optics and has given rise to a rich variety of physical phenomena based on the appearance of exceptional points and phase transitions in the eigenvalues of the associated non-Hermitian Hamiltonian [1,2]. In classical wave systems, where the real part of the potential in optics is the refractive index and gain and/or loss is analogous to its imaginary part and $\mathcal{PT}$-symmetry demands that $n(r) = n^*(-r)$, one can envisage various structures obtained by combining the index and gain and/or loss modulations with required symmetries which represent classical analogs of quantum systems described by $\mathcal{PT}$-symmetric potentials. The recent experimental realizations of $\mathcal{PT}$-symmetric optical systems have attracted widespread interest, in particular due to their promising prospect to achieve tunable components with extreme sensitivity and very unconventional wave behavior [3–6]. These include loss induced invisibility [7], Bloch oscillations [8], laser generation by reversing the effect of loss at threshold [9–11], unidirectional propagation [12,13], and optical solitons in $\mathcal{PT}$ periodic systems [14,15], to name a few of numerous new concepts proposed.

The key feature of $\mathcal{PT}$ symmetric photonic structures stems from the fact that they may have real eigenvalues despite having gain and loss which break the space symmetry. For a certain amount of gain and/or loss, there exists a threshold at which the system undergoes a spontaneous $\mathcal{PT}$-symmetry breaking, and above which eigenfrequencies become complex and power grows exponentially. Based on the $\mathcal{PT}$ concept several types of extended systems included $\mathcal{PT}$ gratings, $\mathcal{PT}$ lattices, and $\mathcal{PT}$-symmetric resonant structures characterized by the complex-valued periodic functions have been studied both theoretically and experimentally [16–19]. The periodic systems also provide asymmetric response, offering for example a unidirectional invisibility [7], unidirectional coupling [20], and other peculiar effects. Due to periodicity such systems are resonant, i.e., provide the asymmetric responses in the vicinity resonant wavelength $\lambda \sim 2a$, where $a$ is the period of the structure.

Most of the $\mathcal{PT}$ studies focus on one-dimensional systems. A naive extension to two dimensions is possible by considering parity symmetry in one space direction, which however can hardly lead to principally novel effects. Some exception is perhaps in [20], where the nontrivial chiral-$\mathcal{PT}$ concept has been introduced, which is possible only in two-dimensional (2D) or 3D systems. The majority of the studies also consider the global $\mathcal{PT}$ symmetry. This means that the bulk is uniformly filled by a continuous $\mathcal{PT}$ media (i.e., by $\mathcal{PT}$ lattices). Perhaps a single exception within this context is the work in [21], where the local-$\mathcal{PT}$ concept has been introduced, providing the $\mathcal{PT}$ effect in different directions. This results in $\mathcal{PT}$ systems with nontrivial flows, i.e., for instance axisymmetric flows toward some focus as suggested in an original proposal [21]. Moreover, it could be extended to build a system with arbitrary $\mathcal{PT}$ flows, like closed loops of currents, chiral objects, and any other flow configuration on demand [22].

The most natural way of looking into the physical properties of such complicated $\mathcal{PT}$ objects is to consider them as structures built from microscopic $\mathcal{PT}$ objects, i.e., so-called $\mathcal{PT}$ molecules represented by $\mathcal{PT}$ dipoles, which can be described as a generalized form of the conventional ones—see Fig. 1. The main idea behind our paper is to identify the $\mathcal{PT}$ dipole as a minimum unit building block which possesses the $\mathcal{PT}$ properties. We demonstrate that such a minimum object consists of two scatterers with different complex scattering coefficients. Realization of $\mathcal{PT}$ symmetry in optics requires that considerable amounts of gain loss can be provided only by semiconductors and polymers. For example, $\mathcal{PT}$-symmetry breaking was observed experimentally in a passive $\mathcal{PT}$-symmetry ridge optical waveguide consisting of multilayer $Al_xGa_{1-x}As$ heterostructure with varying concentration, where the loss is introduced through deposition of a thin layer of chromium on one of the coupler arms [6]. Another configuration employing the $\mathcal{PT}$ symmetry concept was demonstrated in the $\mathcal{PT}$-synthetic microring resonator with InGaAsP multiple quantum wells deposited on InP substrate where balanced gain and/or loss modulation is achieved by periodically formed Cr/Ge structures on the top of the InGaAsP [16]. A possible design of the $\mathcal{PT}$ dipole that could be implemented and measured in microphotonic devices was proposed in the context of 2D $\mathcal{PT}$-symmetric complex structure [20]. The configuration shown in Fig. 4(a) in Ref. [20] consists of a dielectric slab with holes filled by p/n and n/p semiconductor junctions which

 

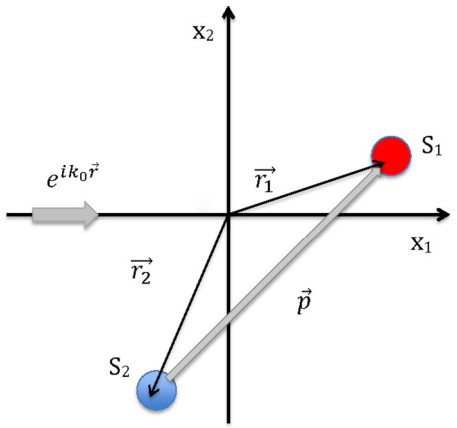


FIG. 1. Single $\mathcal{PT}$ dipole.

provide gain or loss depending on the orientation of each component.

Our paper is organized as follows. In Sec. II we develop a scattering theory of a $\mathcal{PT}$ dipole within the first Born approximation and define the difference in intensity of scattered field between the configurations with $\mathcal{PT}$ dipoles parallel ($\vec{p}$) and antiparallel ($-\vec{p}$) to the direction of the incident wave. We consider two specific configurations of the $\mathcal{PT}$ dipole aligned parallel and perpendicular with respect to the incident wave. In Sec. III we numerically investigate the scattering properties of the $\mathcal{PT}$ dipole represented by the system consisting of infinitely long, parallel cylinders with the opposite sign of the imaginary component of the refractive index. In Sec. IV we present the numerical results for both configurations of the $\mathcal{PT}$ dipole considered. The discussion of the validity of the theoretical model based on the first Born approximation and deviations identified by numerical approach are discussed in Sec. V.

## II. THEORETICAL MODEL

### A. Model

The $\mathcal{PT}$ dipole consists of two point scatterers centered at the positions $\vec{r}_1$ and $\vec{r}_2$ in the $xy$ plane with different complex scattering coefficients $s_1$ and $s_2$—see Fig. 1. The distance between two scatterers, $a = |\vec{r}_1 - \vec{r}_2|$, defines the length scale of the model. Scattering coefficients which represent effective polarizabilities can be in general complex,

$$s_{1,2} = S_{\mathrm{Re}} \pm i S_{\mathrm{Im}}. \tag{1}$$

The real component corresponds to elastic scattering and the imaginary one accounts for the emission and absorption, respectively. The incident field is the plane wave propagating in the $xy$ plane with unit amplitude and normalized frequency $f = a/\lambda$.

### B. Electromagnetic response of the $\mathcal{PT}$ dipole

The total electric field $E$ at a point $\vec{r}$ is assumed to be parallel to the $z$ axis and can be written as a superposition of incident plane wave with unit amplitude and field $E_S$ scattered by two scatterers:

$$E(\vec{r}) = e^{i\vec{k}_0\vec{r}} + E_S(\vec{r}). \tag{2}$$

Here, $k_0 = 2\pi/\lambda$ is the wave vector of the incident wave.

In the limit of weak scattering one can use the first Born approximation which allows one to calculate the field far away from the scattering center. To describe the behavior of a single dipole consisting of two point scatterers we focus on the scattered field that can be written as

$$E_{\mathrm{S}}(\vec{r}) = \sum_{j=1}^{2} \frac{i s_j e^{i\vec{k}_0\vec{r}_j} e^{i|\vec{k}_0||\vec{r}-\vec{r}_j|}}{|\vec{r}-\vec{r}_j|^{1/2}}. \tag{3}$$

In order to obtain analytical insight we first simplify the general expression for the scattered field into asymptotic form in the far-field limit assuming $|\vec{r}| \gg |\vec{r}_{1,2}|$

$$E_{\mathrm{S}}(\vec{r}) = \frac{i\, e^{i|\vec{k}_0||\vec{r}|}}{|\vec{r}|^{1/2}} \left( \sum_{j=1}^{2} s_j e^{i|\vec{k}_0|(\vec{e}_k - \vec{e}_r)\vec{r}_j} + O(|\vec{r}|^{-1}) \right), \tag{4}$$

where unit vectors $\vec{e}_k = \vec{k}_0/|\vec{k}_0|$ and $\vec{e}_r = \vec{r}/|\vec{r}|$ indicate directions of the incident wave and of the observer at the point $\vec{r}$, respectively.

To understand how the $\mathcal{PT}$ symmetry influences the electromagnetic response of the dipole, we first consider the limit of "small" dipole $k_0 a \ll 1$; the latter equation can be simplified into the form

$$E_{\mathrm{S}}(\vec{r}) = \frac{i\, e^{i|\vec{k}_0||\vec{r}|}}{|\vec{r}|^{1/2}} (s + i(\vec{e}_k - \vec{e}_r)\vec{p} + O(|\vec{r}|^{-1})). \tag{5}$$

The first term in the bracket in the latter equation represents the total scattering defined as a sum of the scattering coefficients associated with each of the scatterers $s = \sum_j s_j$. This term is parity-invariant and thus provides symmetric scattering, while the second term in which

$$\vec{p} = |\vec{k}_0| \sum_j s_j \cdot \vec{r}_j \tag{6}$$

defines the $\mathcal{PT}$ dipole and gives rise to asymmetry of scattering which depends on both its strength and orientation.

The parity asymmetry of the scattering can be determined by calculating the scattered field for the dipoles with opposite orientations $\vec{p}$ and $-\vec{p}$. Specifically, in the forward direction $\vec{e}_k = \vec{e}_r$ when orientation of the dipole coincides with the direction of the incident wave, the second term in the brackets of Eq. (5) vanishes and the scattered field does not depend on the $\mathcal{PT}$ dipole $\vec{p}$. In the case of backward scattering when $\vec{e}_k = -\vec{e}_r$ the scattered field given by Eq. (5) is proportional to $s + 2i\vec{e}_k\vec{p}$. This means that for real-valued scalar scattering $s = \sum_j s_j$ and for real-valued $\mathcal{PT}$ dipole $\vec{p}$ the parity symmetry is maintained, i.e., $|s + 2i\vec{e}_k\vec{p}| = |s - 2i\vec{e}_k\vec{p}|$. On the other hand, when the scattering is described in terms of the complex coefficients $s_j$, the parity symmetry is broken. Thus asymmetric scattering requires the dipole characterized by nonzero elastic scattering and a nonzero gain and/or loss balance.

The preceding discussion is valid also without assumption of "small" dipoles. In what follows the condition $k_0 a \ll 1$ is lifted. By using the notation $\vec{r}_{1,2} = \pm\Delta\vec{r}/2$, Eq. (4) can be

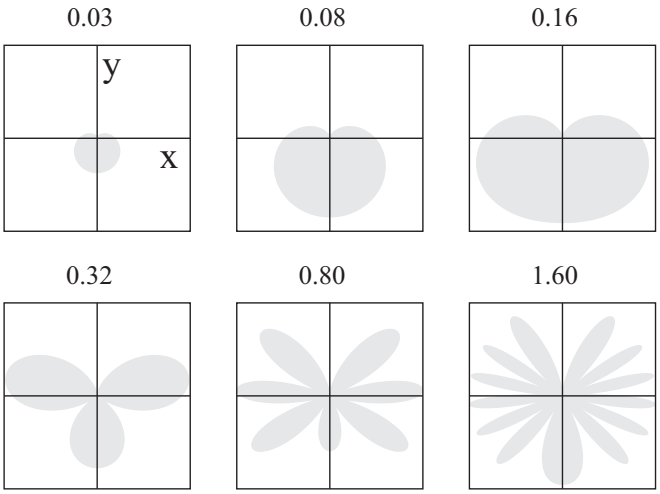


FIG. 2. Angular diagrams of $\mathcal{PT}$ asymmetry $\Delta P_S(\vec{r})$ in the case of parallel orientation of the $\mathcal{PT}$ dipole for the normalized frequencies $f = a/\lambda = k_0 a/(2\pi)$ in the range $0.03 < f < 1.6$. Incident wave propagates along the $y$ axis. Orientation of axes is shown in the left upper panel. Since all panels have the same scale, diagrams give also an estimation how the total scattered energy depends on the frequency of incident wave.

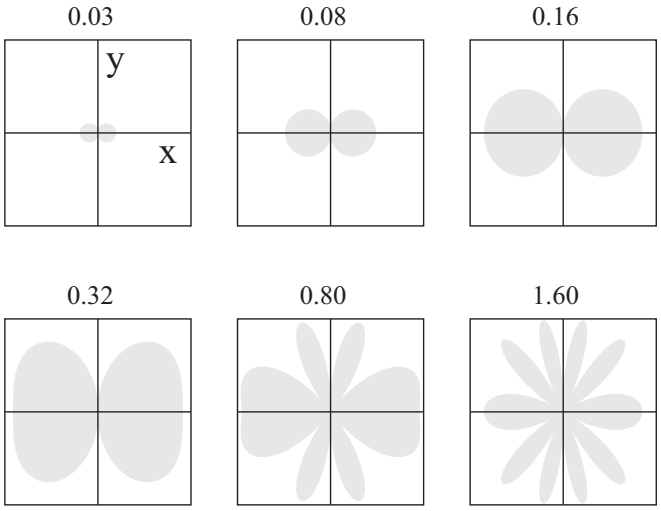


FIG. 3. Same as in Fig. 2 but for perpendicular orientation of the $\mathcal{PT}$ dipole.

rewritten into the form

$$E_S(\vec{r},\vec{p}) = \frac{2i\, e^{i|k_0||\vec{r}|}}{|\vec{r}|^{1/2}}\left[S_{\mathrm{Re}}\cos\left(\frac{|\vec{k}_0|(\vec{e}_k-\vec{e}_r)\cdot\Delta\vec{r}}{2}\right) + S_{\mathrm{Im}}\sin\left(\frac{|\vec{k}_0|(\vec{e}_k-\vec{e}_r)\cdot\Delta\vec{r}}{2}\right)\right], \tag{7}$$

according to which the $E_S(\vec{r},\vec{p})$ depends on the orientation of the dipole. To characterize the asymmetry of scattered field associated with the opposite orientations of the $\mathcal{PT}$ dipole, we calculate the difference in the intensity of scattered field between the configurations with $\mathcal{PT}$ dipoles aligned parallel and antiparallel to the direction of the incident wave:

$$\Delta P_S(\vec{r}) = ||E_S(\vec{r},\vec{p})|^2 - |E_S(\vec{r},-\vec{p})|^2|. \tag{8}$$

We apply expressions (7) and (8) to the following two specific orientations of the dipole.

When the $\mathcal{PT}$ dipole is oriented along the direction of the incident wave, $\vec{e}_k \parallel \Delta\vec{r}$, the scattering field can be expressed as a function of the observation angle $\theta$,

$$E_S(\vec{r}) = \frac{2i\, e^{i|k_0||\vec{r}|}}{|\vec{r}|^{1/2}}\left[S_{\mathrm{Re}}\cos\left(\frac{k_0 a(1-\cos\theta)}{2}\right) + S_{\mathrm{Im}}\sin\left(\frac{k_0 a(1-\cos\theta)}{2}\right)\right], \tag{9}$$

where $\cos\theta = \vec{e}_k\cdot\vec{r}/|\vec{r}|$, and

$$\Delta P_S(\vec{r}) = \frac{4S_{\mathrm{Re}}S_{\mathrm{Im}}}{|\vec{r}|}\sin[k_0 a(1-\cos\theta)]. \tag{10}$$

The behavior of the angular dependence of $\Delta P_S(\vec{r})$, given by Eq. (10), is demonstrated in Fig. 2. The forward scattering does not depend on the orientation of the dipole [$\Delta P_S(\theta = 0) = 0$], while significant asymmetry is observed in the backward scattering ($\theta = \pi$). Interestingly, the backward scattering is symmetric in special cases when $2ak_0 = \pi N$, where $N$ is an integer, i.e., an "accidental" symmetric backscattering occurs at the wavelengths $\lambda_N = 4a/N$.

In the case when the $\mathcal{PT}$ dipole is oriented perpendicular to the direction of the incident wave, $\vec{e}_k \perp \Delta\vec{r}$, the scattering field can be expressed as a function of the observation angle $\theta$,

$$E_S(\vec{r}) = \frac{2i\, e^{i|k_0||\vec{r}|}}{|\vec{r}|^{1/2}}\left[S_{\mathrm{Re}}\cos\left(\frac{k_0 a\,\sin\theta}{2}\right) - S_{\mathrm{Im}}\sin\left(\frac{k_0 a\,\sin\theta}{2}\right)\right], \tag{11}$$

and the asymmetry in the scattered field between the opposite orientation of the $\mathcal{PT}$ dipole reads

$$\Delta P_S(\vec{r}) = \frac{4S_{\mathrm{Re}}S_{\mathrm{Im}}}{|\vec{r}|}\sin(k_0 a\sin\theta). \tag{12}$$

One can see in this case that no asymmetry between forward ($\theta = 0$) and backward ($\theta = \pi$) scattering occurs. In addition, Eq. (12) allows one to determine the critical observation angle $\theta$ at which the asymmetry $\Delta P_S(\vec{r})$ vanishes for a given frequency $f$: $\theta = \arcsin(N/(2f))$ and yields a number of the critical observation angles $N_\theta$ which appear in one quadrant for the frequencies $f > N_\theta/2$. These features arising from Eq. (12) can be observed in the angular dependence of $\Delta P_S(\vec{r})$ shown in Fig. 3.

Equations (7) and (8) allow us to evaluate both frequency and angular dependence of the asymmetry scattering of the $\mathcal{PT}$ dipole and could be generalized for arbitrary orientation of the dipole. As expected, the scattered field decreases as $r^{-1}$ at large distances. The only parameter which determines the angular dependence of the scattered field is $k_0 a = 2\pi a/\lambda$.

## III. NUMERICAL METHOD

In numerical calculation, the $\mathcal{PT}$ dipole is represented by two infinitely long cylinders, parallel to the $z$ axis. The

distance between centers of the cylinders is $a$. The radius of cylinders is $R_0$ and refractive indices $n_j = n_R \pm i n_I$, $j = 1,2$. The incident electromagnetic plane wave with normalized frequency $f = a/\lambda$ propagating in the $xy$ plane

$$E(x,y|\omega)_{\text{inc}} = \exp[i(k_x x + k_y y) - i\omega t] \tag{13}$$

is polarized parallel to the axes of cylinders.

The total electric field can be expressed as the sum of the incident field $E(x,y|\omega)_{\text{inc}}$ and a scattered field $E_S(x,y|\omega)$

$$E(x,y|\omega) = E(x,y|\omega)_{\text{inc}} + E_S(x,y|\omega). \tag{14}$$

To study scattering properties of EM waves for a single $\mathcal{PT}$ dipole we evaluate the radial component of the Poynting vector

$$P_S(R,\phi) = E_S(R,\phi)[H_S^{\phi}(R,\phi)]^* \tag{15}$$

along the circumference of the circle with radius $R$ centered at the focus of the system. In Eq. (15),

$$H_S^{\phi} = \frac{i}{\omega\mu}\frac{\partial E_S}{\partial r}\bigg|_{r=R} \tag{16}$$

is the tangential component of magnetic field.

In analogy to Eq. (8) we characterize the asymmetry of scattered field associated with the opposite orientation of the $\mathcal{PT}$ dipole in terms of the difference $\Delta P_S(R,\phi)$ defined as

$$\Delta P_S(R,\phi) = |P_S(R,\phi,\vec{p}) - P_S(R,\phi,-\vec{p})|. \tag{17}$$

To compute the $\Delta P_S(R,\phi)$ we apply a numerical algorithm based on the expansion of electromagnetic field into cylinder functions [23]. The scattered electric field can be expressed in cylindrical coordinates $r$ and $\phi$ as

$$E_S^j(\vec{r}) = \sum_{j=1}^{2}\sum_m \beta_m^j H_m(k_0|\vec{r} - \vec{r}_j|)e^{im\phi_j}, \tag{18}$$

where $H_m$ are the Hankel functions of the first kind and $r_j$, $\phi_j$ are cylinder coordinates centered at the center of the $j$th cylinder. The coefficients $\beta_m$ can be calculated from the continuity condition of the tangential components of the electric and magnetic field at the boundary of cylinders. Our approach is described in detail in Refs. [24,25].

## IV. RESULTS

### A. $\mathcal{PT}$-dipole–parallel configuration

We first consider the case when the $\mathcal{PT}$ dipole is parallel to the propagation direction of the incident wave. The system which represents a $\mathcal{PT}$ dipole consists of two cylinders of radius $R_0 = 0.1a$ characterized by the refractive index $n_i = n_R \pm i n_I$, $i = 1,2$, where the real part $n_R = 3.5$ is kept constant while an imaginary part is varied in the range $0.005 < n_I < 0.5$. We have chosen the radius of the cylinder to be sufficiently small $R_0 = 0.1a$ to allow comparison with analytic results based on the point scatterer approximation. In Fig. 4, we display the scattering diagrams obtained for the frequency $f = 0.16$ for two of the parallel orientations of the dipole $\pm\vec{p}$ in the near-field ($R = 2a$) and far-field limit ($R = 20a$). The gray shaded area in Fig. 4 which shows the absolute value of the difference between the scattered power $\Delta P_S(R,\phi)$ for both orientations $\vec{p}$ and $-\vec{p}$ represents the key

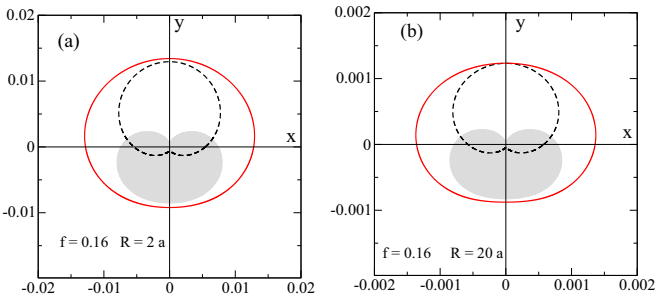


FIG. 4. Intensity of scattered field for two opposite orientations of the dipole parallel to the propagation of the incident wave (dashed black and solid red lines) and their difference $\Delta P_S(R,\phi)$ (shaded area) for the $\mathcal{PT}$ dipole with gain and/or loss characterized by $n_I = \pm 0.5i$. (a) In the near field ($R = 2a$) and (b) in the far field ($R = 20a$). The frequency of an incident wave $f = 0.16$.

feature associated with scattering properties of the $\mathcal{PT}$ dipole. Primarily, in the case of parallel orientation of the $\mathcal{PT}$ dipole the scattering diagrams reveal a strong asymmetry along the direction of propagation of the incident wave. Such a behavior is consistent with analytical results given by Eq. (10) and it is displayed in Fig. 2. In addition, one can observe that in the far field the power scattered along the $y$ axis for two antiparallel orientations of the dipole shown in Fig. 4(b) coincide and yield a vanishing difference $\Delta P_S(R,\phi = 0)$. Simultaneously, this behavior confirms the theoretical prediction given by Eq. (5). By inspecting the scattering of the $\mathcal{PT}$ dipole in the near-field limit we found the asymmetry of the transmitted power along $y$ axis as it is demonstrated in Fig. 4(a). We explored the existence of this phenomenon also at larger frequencies where the system reveals according to the theoretical model richer scattering patterns (Fig. 2). As an example, we display in Fig. 5 the scattering diagram for the frequency $f = 1$.

To quantify the transition between the near- and far-field limit we depict in Fig. 6 the dependence of the field scattered along the $y$ axis on the normalized radius $R/a$ for both orientations of the dipole. One can see that the asymmetry in the forward scattering vanishes at $R \simeq 12.5a$ which suggests that the nonvanishing difference in the forward scattering appears solely in the near-field regime. Since scattered fields decrease as $\sim 1/R$ in the far field, the normalized product

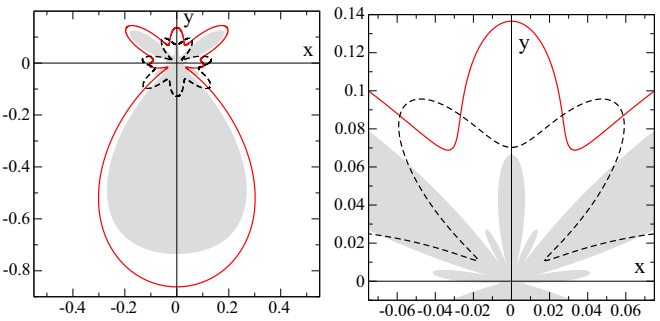


FIG. 5. Left: the difference in the intensity scattering for two antiparallel orientations of $\mathcal{PT}$ dipole $\Delta P_S(R,\phi)$ characterized by $n_I = \pm 0.5i$ in the near field ($R = 2a$). Right panel shows the detail of the scattered field. The frequency of an incident wave $f = 1.0$.

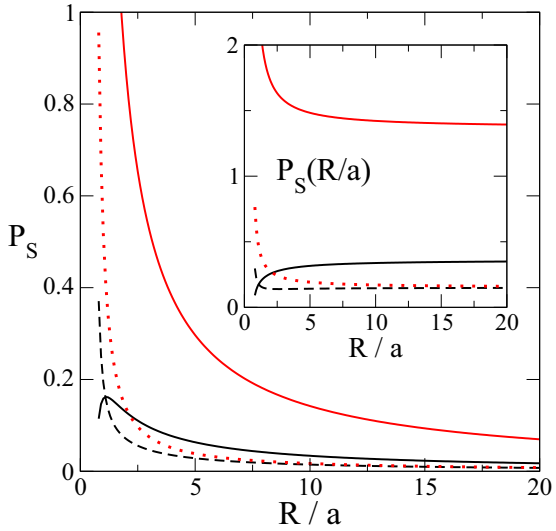


FIG. 6. Intensity of the scattered field $P_S(R,\phi)$ along the $y$ axis as a function of the normalized radius $R/a$. Solid lines represent backward scattering for two orientations of the dipole. Similarly, black dashed and red dotted lines show the forward scattering for two antiparallel orientations of the dipole. Inset shows the product $P_S(R/a)$ to prove that the intensity of scattered field decreases $\sim 1/R$ in the far field.

$RP/a$ remains constant for the backward scattering as it is shown in the inset of Fig. 6.

Besides the effect associated with near-field asymmetry described above, we found yet another interesting difference between the theoretical prediction and numerical results. Namely, we observed that the scattering pattern associated with a $\mathcal{PT}$ dipole in the far-field limit obtained numerically reveals strong dependence on the strength of the imaginary part $n_I$. It is demonstrated in Fig. 7, where dependencies of the scattering diagrams for three values of the gain and/or loss parameters are depicted. We note that, according to the theoretical model of the difference between the intensities for antiparallel orientations of the $\mathcal{PT}$ dipole given by Eq. (10), the size of the imaginary component $n_I$ does not affect the shape

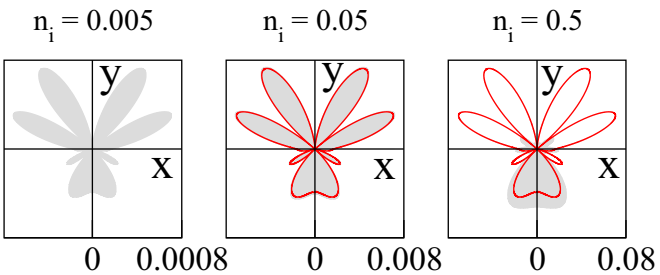


FIG. 7. Difference in the intensity scattering for antiparallel orientations of $\mathcal{PT}$ dipole $\Delta P_S(R,\phi)$ in the far field ($R = 20$) vs gain and/or loss parameter $n_I = \pm 0.005i$ (left), $n_I = \pm 0.05i$ (middle), and $n_I = \pm 0.5i$ (right), when $f = 1.0$. Red line in the middle (right) panel represents $\Delta P_S$ from the left (middle) panels, respectively, multiplied by a factor of 10, to display a linear dependence of scattered intensity on the gain and/or loss parameter $n_I$ for small values $n_I$ and its breaking when $n_I$ increases.

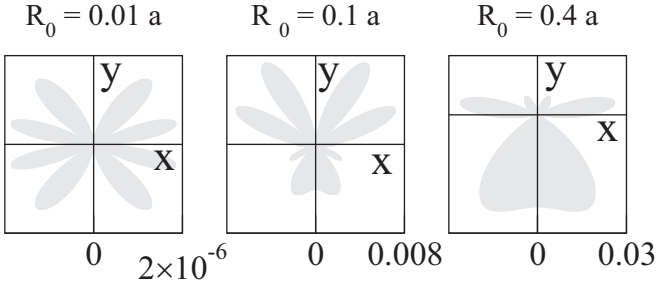


FIG. 8. Difference in the intensity scattering for antiparallel orientations of the $\mathcal{PT}$ dipole $\Delta P_S(R,\phi)$ in the far field ($R = 20$) vs radius of the cylinder for $n_I = \pm 0.05i$, $R_0 = 0.01a$ (left), $R_0 = 0.1a$ (middle), and $R_0 = 0.4a$ (right). The frequency $f = 1.0$. Note that Born approximation predicts the symmetrical backscattering for this frequency. Numerically, this is observed only for very tiny cylinders (the left panel). For stronger scatterers, Born approximation is not valid.

of $\Delta P_S(R,\phi)$. The theoretical approach in principle cannot account for the features described above.

To quantify the range of the gain and/or loss parameter beyond which the numerical results indicate limits of the validity of the Born approximation we compare in the middle panel of Fig. 7 the scattering intensities for two values of $n_I$: 0.005 (red line, multiplied by 10) and $n_I = 0.05$. Clearly, the scattering increase linearly with $n_I$ for small values of $n_I$. The same procedure applied to the results for $n_I = 0.05$ and 0.5 (right panel of Fig. 7) unveils the breaking of linear behavior for higher gain and/or loss parameter.

For completeness, we also studied how the scattering pattern is affected when the radius of the cylinder is varied in the range $0.01a < R_0 < 0.4a$—see Fig. 8. One can observe that in comparison with the results shown in Fig. 7 which display the dependence of the $\Delta P_S(R,\phi)$ on the $n_I$, the variation of the radius gives rise to a significantly wider range of the $\Delta P_S(R,\phi)$ and to a strong dependence of the shape of the scattering pattern. We do not expect any simple $R_0$ dependence of the scattering pattern since the latter is strongly affected by Fano resonances [25,26].

The result shown in the left panel of Fig. 8 confirms the accidental symmetry in the backscattering in the far-field limit along the $y$ axis which occurs for small $\mathcal{PT}$ dipoles. The effect observed in numerical calculations occurs at the integer-valued frequencies at which the difference $\Delta P_S(R,\phi)$ vanishes and is in accord with the theoretical model in the far-field limit given by Eq. (10). This result also indicates that Born approximation is not sufficient for thicker cylinders as shown in the middle and the right panels of Fig. 8, where the backscattering is not symmetric.

### B. $\mathcal{PT}$-dipole–perpendicular configuration

In Fig. 9 we show the scattering patterns in the near-field limit ($R = 2a$) for the perpendicular orientation of the $\mathcal{PT}$ dipole for two different frequencies. The intensity of the scattered power $\Delta P_S(R,\phi)$ for parallel and antiparallel orientations $\pm\vec{p}$ indicated by dashed black and solid red lines possess the features which significantly deviate from those

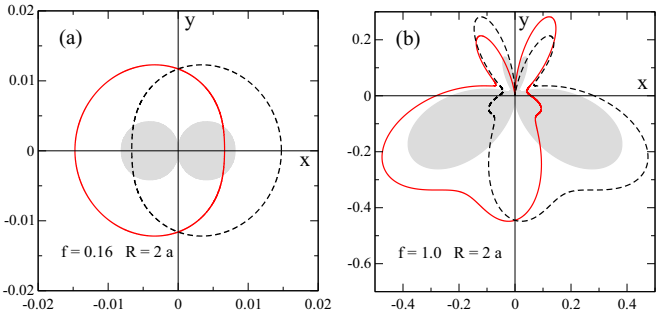


FIG. 9. Difference in the intensity scattering for two antiparallel orientations of $\mathcal{PT}$ dipole lying perpendicular to incident wave (black dashed and red solid line). Dashed area is the difference $\Delta P_S$. Gain and/or loss parameter $n_I = \pm 0.5$. Left: $f = 0.16$; right: $f = 1.0$.

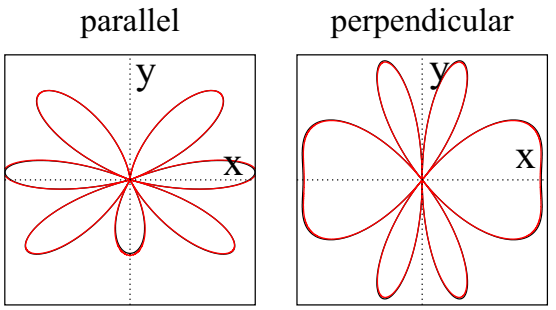


FIG. 11. Angular diagrams of $\mathcal{PT}$ asymmetry for both parallel and perpendicular orientation of the $\mathcal{PT}$ dipole given by $\Delta P_S(R,\phi)$ at frequency $f = 0.8$. Analytical prediction, given by Eq. (10) (black line) is compared with numerical data for $R_0 = 0.01a$, $n_I = 0.005$, and $R = 20a$ (red line, rescaled in absolute value).

associated with parallel orientation of the $\mathcal{PT}$ dipole, while the asymmetric scattering indicated by the shaded areas is maintained. It is interesting to note that for small frequencies the $\Delta P_S(R,\phi)$ is symmetric along both $x$ and $y$ axis while with an increasing frequency becomes strongly asymmetric along the $y$ axis. One can also observe that in contrast to the parallel orientation of the $\mathcal{PT}$ dipole asymmetric scattering does not occur along the $y$ axis in accord with the theoretical model—see Eq. (12).

In Fig. 10 we demonstrate the dependence of the scattering diagrams in the far field for three values of the gain and/or loss parameter $n_I$. The scattering patterns display qualitatively similar behavior as those associated with parallel orientation shown in Fig. 8; in particular they confirm a linear dependence on the gain and/or loss parameter $n_I$ in the range $0.005 < n_I < 0.05$ within the range of the validity of the first Born approximation.

## V. DISCUSSION AND CONCLUSIONS

The numerical results presented in the previous section confirm the asymmetric scattering of the $\mathcal{PT}$ dipole for both parallel and perpendicular dipole orientations and simultaneously offer the possibility to examine the limits of the theoretical model associated with the approximations implemented.

First of all, we numerically explored differences in the scattering patterns arising in the near field which are

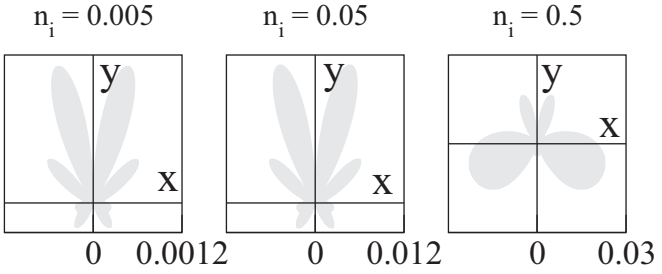


FIG. 10. Dependence of the difference in the intensity scattering for antiparallel orientations of the $\mathcal{PT}$ dipole given by $\Delta P_S(R,\phi)$ in the far field ($R = 20$) on the gain and/or loss parameter for $n_I = \pm 0.005i$ (left), $n_I = \pm 0.05i$ (middle), and $n_I = \pm 0.5i$ (right), when $f = 1.0$.

demonstrated in Figs. 5 and 6, in particular that in the near field the scattering in the forward direction ceases to be symmetric. This feature clearly arises due to the modified properties of the scattering pattern when the transition between the near- and far-field limit takes place as shown in Fig. 6 and yields the threshold between both regimes.

To check the validity of the Born approximation we compare the results obtained analytically and numerically for the case of small $\mathcal{PT}$ dipole with the radius $R = 0.01a$ and gain and/or loss parameter $n_I = 0.005$—see Fig. 11. The analytical and numerical results coincide for both orientations of the $\mathcal{PT}$ dipole.

In addition, the limit of the validity of the first Born approximation has been determined by exploring the dependence of the scattering of the $\mathcal{PT}$ dipole on the size of the gain and/or loss parameter $n_I$. We have shown that when the size of the imaginary component $n_I$ is small ($\lesssim 0.05$) it does not qualitatively affect the shape of $\Delta P_S(R,\phi)$ and follows the linear dependence on $n_I$ in accord with the first Born approximation. When the size of the $n_I$ is increased, the linear scaling of the scattering with the $n_I$ does not apply and the system cannot be described in terms of the first Born approximation. Finally, we note that the results shown in Fig. 9 which demonstrate the dependence of the $\Delta P_S(R,\phi)$ display the strong dependence on the radius of the cylinder $R_0$; however, one cannot anticipate any trivial scaling since its behavior may be strongly affected for the frequencies in the vicinity of the Fano resonances.

In conclusion, we analyzed, both analytically and numerically, the electromagnetic response of the $\mathcal{PT}$ dipole and found that the Born approximation is valid in the limit of far field and tiny scattering parameters of the dipole. For a general case, rich variety of the scattering pattern is observed both for the parallel and perpendicular orientation of the dipole. Our results indicate that structures composed from a large number of $\mathcal{PT}$ dipoles might possess interesting transmission properties, worth analyzing in the future.

## ACKNOWLEDGMENTS

K.S. acknowledges financial support of NATO SPS research Grant No. 985048, support from Spanish Ministerio de Ciencia e Innovación, and European Union FEDER through

Project No. FIS2015-65998-C2-1-P. The research of P.M. was supported by the Slovak Research and Development Agency under Contract No. APVV-15-0496 and by the Agency VEGA under Contract No. 1/0108/17. The research of V.K. was supported by Grant No. 16-00329S of the Czech Science Foundation (CSF).

[1] C. M. Bender and S. Boettcher, Phys. Rev. Lett. **80**, 5243 (1998).
[2] C. M. Bender, Rep. Prog. Phys. **70**, 947 (2007).
[3] For a recent review see, for example, PT Symmetry in Optics and Photonics, focus issue of New. J. Phys. **19** (2017); http://iopscience.iop.org/journal/1367-2630/page/Focus%20on%20Parity-Time%20Symmetry%20in%20Optics%20and%20Photonics.
[4] A. Ruschhaupt, F. Delgado, and J. G. Muga, J. Phys. A **38**, L171 (2005).
[5] K. G. Makris, R. El-Ganainy, D. N. Christodoulides, and Z. H. Musslimani, Phys. Rev. Lett. **100**, 103904 (2008).
[6] A. Guo, G. J. Salamo, D. Duchesne, R. Morandotti, M. Volatier-Ravat, V. Aimez, G. A. Siviloglou, and D. N. Christodoulides, Phys. Rev. Lett. **103**, 093902 (2009).
[7] Z. Lin, H. Ramezani, T. Eichelkraut, T. Kottos, H. Cao, and D. N. Christodoulides, Phys. Rev. Lett. **106**, 213901 (2011).
[8] S. Longhi, Phys. Rev. Lett. **103**, 123601 (2009).
[9] B. Peng *et al.*, Science **346**, 328 (2014).
[10] M. Brandstetter *et al.*, Nat. Commun. **5**, 4034 (2014).
[11] S. Phang *et al.*, Opt. Express **23**, 11493 (2015).
[12] A. Regensburger *et al.*, Nature (London) **488**, 167 (2012).
[13] L. Feng *et al.*, Nat. Mater. **12**, 108 (2013).
[14] Z. H. Musslimani, K. G. Makris, R. El-Ganainy, and D. N. Christodoulides, Phys. Rev. Lett. **100**, 030402 (2008).
[15] M. Wimmer *et al.*, Nat. Commun. **6**, 7782 (2015).
[16] L. Feng *et al.*, Science **346**, 972 (2014).
[17] S. Longhi, Phys. Rev. A **82**, 031801 (2010).
[18] H. Hodaei *et al.*, Science **346**, 975 (2014).
[19] S. Phang *et al.*, Sci. Rep. **6**, 20499 (2016).
[20] M. Turduev, M. Botey, I. Giden, R. Herrero, H. Kurt, E. Ozbay, and K. Staliunas, Phys. Rev. A **91**, 023825 (2015).
[21] W. W. Ahmed, R. Herrero, M. Botey, and K. Staliunas, Phys. Rev. A **94**, 053819 (2016).
[22] W. W. Ahmed, R. Herrero, M. Botey, and K. Staliunas, arXiv:1707.04556.
[23] H. C. van de Hulst, *Light Scattering by Small Particles* (Dover, New York, 1981).
[24] P. Markoš, Opt. Commun. **361**, 65 (2016).
[25] P. Markoš, Phys. Rev. A **92**, 043814 (2015).
[26] M. V. Rybin, D. S. Filonov, P. A. Belov, Y. S. Kivshar, and M. F. Limonov, Sci. Rep. **5**, 8774 (2015).